

Towards an efficient algorithm for the simulation of viscous two-phase flows with real gas effects

Remi Abgrall, Maria Giovanna Rodio, Pietro Marco Congedo

▶ **To cite this version:**

Remi Abgrall, Maria Giovanna Rodio, Pietro Marco Congedo. Towards an efficient algorithm for the simulation of viscous two-phase flows with real gas effects. [Research Report] RR-8173, INRIA. 2012. hal-00762841

HAL Id: hal-00762841
https://inria.hal.science/hal-00762841

Submitted on 8 Dec 2012

HAL is a multi-disciplinary open access archive for the deposit and dissemination of scientific research documents, whether they are published or not. The documents may come from teaching and research institutions in France or abroad, or from public or private research centers.

L'archive ouverte pluridisciplinaire **HAL**, est destinée au dépôt et à la diffusion de documents scientifiques de niveau recherche, publiés ou non, émanant des établissements d'enseignement et de recherche français ou étrangers, des laboratoires publics ou privés.

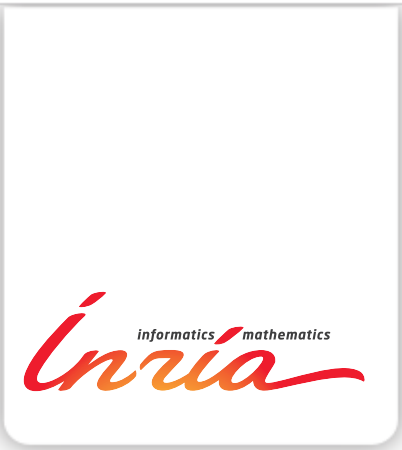


Towards an efficient algorithm for the simulation of viscous two-phase flows with real gas effects

Remi Abgrall, Maria Giovanna Rodio, Pietro Marco Congedo

RESEARCH REPORT
N° 8173
December 8, 2012
Project-Team Bacchus

ISSN 0249-6399 ISRN INRIA/RR--8173--FR+ENG



Towards an efficient algorithm for the simulation of viscous two-phase flows with real gas effects

Remi Abgrall, Maria Giovanna Rodio, Pietro Marco Congedo

Project-Team Bacchus

Research Report n° 8173 — December 8, 2012 — 26 pages

Abstract: A discrete equation method (DEM) for the simulation of compressible multiphase flows including viscous and real-gas effects is illustrated. A reduced five equation model is obtained starting from the semi-discrete numerical approximation of the two-phase viscous model. Then, a simple algorithm is proposed in order to use two different equations of state at the vapor and liquid-vapor conditions. Simulation results are validated with well-known results in literature. Potentialities in improving the quality of the numerical prediction by using a more complex equation of state are thus drawn.

Key-words: DEM method, two-phase flows, Peng-Robinson equation of state, Stiffened Gas equation of state, shock tube.

RESEARCH CENTRE
BORDEAUX – SUD-OUEST

351, Cours de la Libération
Bâtiment A 29
33405 Talence Cedex

Vers la construction d'un algorithme efficace pour la simulation des ecoulements visqueux diphasiques prenant en compte des effets de gaz réel

Résumé : Une méthode de type DEM pour la simulation des écoulements multiphasiques compressibles incluant les effets de viscosité et de gaz réel est proposée. Un modèle réduit à 5 équations est obtenu en partant d'une approximation numérique du modèle visqueux diphasique. Ensuite, un algorithme est décrit qui permet d'utiliser deux équations d'état différentes pour prendre en compte les conditions de la vapeur et du mélange liquide-vapeur. Les résultats de la simulation sont validés avec des solutions de référence connues en littérature. L'intérêt à utiliser des équations d'état plus complexes et précises est montré avec plusieurs cas-tests.

Mots-clés : Méthode DEM, écoulements diphasiques, équation d'état de Peng-Robinson, équation d'état de type Stiffened, tube à choc.

1 Introduction

Modeling two-phase flows is of primary importance for engineering applications. Two aspects are fundamental: (i) how to model the interface between two fluids with different thermodynamic properties and (ii) to characterize the mechanisms occurring at the interface as well as in zones where the volume fractions are not uniform. Several methods have been proposed to model the interface time evolution and reconstruction as in *Lagrangian methods*, *Arbitrary Lagrangian-Eulerian methods (ALE)*, the *Level set method*, *etc.* [1, 2, 3] or to deal with the interface as a diffusion zone, for which consistent thermodynamic equations should be considered [4, 5, 6, 7].

Instead of the traditional approaches to multiphase modeling, where an averaged system of (ill-posed) partial differential equations (PDEs) discretized to form a numerical scheme are considered, the discrete equation method (DEM) results in well-posed hyperbolic systems. This allows a clear treatment of non-conservative terms (terms involving interfacial variables and volume fraction gradients) permitting the solution of interface problems without conservation errors. This method displays several advantages, such as an accurate computation of transient flows as the model is unconditionally hyperbolic, boundary conditions solved with a simple and accurate treatment, an accurate computation of non-equilibrium flows as well as flows evolving in partial or total equilibrium. With the DEM, each phase is compressible and behaves according to a convex equation of state (EOS). In many works of interface problem, the *Stiffened Gas* (SG) EOS was usually used [8, 6, 9, 10]. As explained in Saurel *et al.* [11, 12], this EOS allows an explicit mathematical calculations of important flow relation thanks to its simple analytical form. Moreover, in mass transfer problem it assures the positivity of speed of sound in the two-phase region, under the saturation curve.

When complex fluids are considered, such as cryogenic, molecularly complex and so on, the use of simplex EOS can produce imprecise estimation of the thermodynamic properties, thus deteriorating the accuracy of the prediction. Increasing the complexity of the model and calibrating the adding parameters with respect to the available experimental data constitutes a valid option for saving the good prediction of the model. Nevertheless, it could be very challenging because of the numerical difficulties for the implementation of more complex mathematical model and because of the large uncertainties that generally affected the experimental data.

An effort for developing a more predictive tool for multiphase compressible flows is underway in Bacchus Team (INRIA-Bordeaux). Within this project, several advancements have been performed, *i.e.* considering a more complete systems of equations including viscosity [13], working on the thermodynamic modeling of complex fluids [14, 15], and developing stochastic methods for uncertainty quantification in compressible flows [14, 16]. The aim of this paper is to show how the numerical solver based on a DEM formulation has been modified for including viscous effects and a more complex equation of state for the vapor region. The method used in this paper is the DEM (see [6]) for the resolution of a reduced five equation model with the hypothesis of pressure and velocity equilibrium [17], without mass and heat transfer. This method results in a well-posed hyperbolic systems, allowing an explicit treatment of non conservative terms, without conservation error. The DEM method directly obtains a well-posed discrete equation system from the single-phase conservation laws, producing a numerical scheme which accurately computes fluxes for arbitrary number of phases. The DEM method has been extensively tested in several test cases reproducing unsteady and wave propagation flows [6, 17, 18]. In this paper, two thermodynamic models are considered, *i.e.* the SG EOS and the Peng-Robinson (PR) EOS. While SG allows preserving the hyperbolicity of the system also in spinodal zone, real-gas effects are taken into account by using the more complex PR equation. The higher robustness of the PR equation when coupled with CFD solvers with respect to more complex and potentially more accurate multi-parameter equations of state has been discussed in [19, 20]. In this paper, no

mass transfer effect is taken into account, thus the PR equation can be used only to describe the vapor behavior, while only the SG model is used for describing the liquid.

This paper is organized as follows. In section 2, a description of the reduced five equation model with viscous effects is given. We derive a semi-discrete numerical approximation of the two-phase model. Then, we perform an average procedure of the discrete approximation and an extension to the second-order. Finally, the asymptotic expansion is analyzed to obtain a semi-discrete approximation for a reduced five-equation model. Then, in section 3.1, we describe the SG and PR EOS for the pure fluid and then we derive the thermodynamic properties of mixture, supposing the use of SG EOS for all phase and of PR EOS only for the vapor phase. The section 4 is divided in two parts: in the first one, the implementation of the complex equation of state is validated by reproducing a quasi single-fluid shock tube, *i.e.* considering a very reduced liquid fraction. Then, in the second part, the code is validated against some well-known two-phase test-cases in literature. Finally, the influence of using a more complex equation of state is analyzed by considering several operating conditions in the proximity of the saturation curve.

2 Problem Statement

The present approach is based on a five-equation model with pressure and velocity equilibrium, obtained after an asymptotic analysis in which the relaxation terms disappears. The method for the resolution of a viscous five equation model has been amply developed in [13]. In this work, we give the main lines of the scheme. In this section, let us start by illustrating the reduced model, then the numerical scheme and finally the thermodynamic closure of the system.

2.1 Five equation model

The starting point of the present analysis is a viscous seven equation model composed by the conservative equation for each phase and by the characteristic function X^k of the phase Σ_k. The function $X^k(x,t)$ is equal to 1 if x lies in the fluid Σ_k at time t and 0 otherwise. An averaging procedure similar to that used by Drew [21] is applied to this equation, obtaining the following model:

$$\begin{cases} \dfrac{\partial \bar{\alpha}^k}{\partial t} & = -\mathcal{E}(\sigma \cdot \nabla \bar{\alpha}^k) + \mu_r (P^k - P^{k^*}) \\ \dfrac{\partial \bar{\alpha}^k \bar{\rho}^k}{\partial t} + \nabla(\bar{\alpha}^k \bar{\rho}^k \vec{v}^k) & = \mathcal{E}(\rho_I (\vec{v}_I^k - \sigma) \cdot \nabla X^k) \\ \dfrac{\partial \bar{\alpha}^k \bar{\rho}^k \vec{v}^k}{\partial t} + \nabla(\bar{\alpha}^k \bar{\rho}^k \vec{v}^k \otimes \vec{v}^k + \bar{\alpha}^k \bar{P}^k \mathbb{I}) & = \mathcal{E}\left((\rho_I^k \vec{v}_I^k (\vec{v}_I^k - \sigma) + P_I \mathbb{I}) \cdot \nabla X^k\right) + \\ & \quad + \nabla \cdot (\bar{\alpha}^k \bar{\tau}^k) - \mathcal{E}(\tau_I \cdot \nabla X^k) + \lambda(\vec{v}^{k^*} - \vec{v}^k) \\ \dfrac{\partial \bar{\alpha}^k \bar{\rho}^k \bar{E}^k}{\partial t} + \nabla(\bar{\alpha}^k (\bar{\rho}^k \bar{E}^k \vec{v}^k + \bar{P}^k \mathbb{I} \vec{v}^k) & = \mathcal{E}\left((\rho_I E_I (\vec{v}_I^k - \sigma) + P_I \mathbb{I}) \cdot \nabla X^k\right) + \\ & \quad + \lambda \vec{v}_I^k (\vec{v}^{k^*} - \vec{v}^k) + \mu_r P_I (P^k - P^{k^*}) \\ & \quad + \nabla \cdot (\bar{\alpha}^k (\bar{\tau}^k \cdot \vec{v}_I^k)) - \mathcal{E}((\tau_I \vec{v}^k) \cdot \nabla X^k) \end{cases} \tag{1}$$

where the two phases are indicated with k and k^*; ρ_k, α_k, $\vec{v}^k$ and P_k are the fluid density, the volume fraction, the velocity vector and the pressure for each phase k, respectively; E_k is the total energy of each phase defined as $E^k = \bar{e}^k + \frac{1}{2}\bar{u}_k \cdot \bar{u}_k$. P_I and v_I are the pressure and velocity at the interface of the component k, respectively, defined as:

$$\begin{cases} P_I^k = \frac{Z^k P^{k^*} + Z^{k^*} P^k}{Z^k + Z^{k^*}} + sign\left(\frac{\partial \alpha^k}{\partial x},\right) \frac{(v^{k^*} - v^k)}{Z^k + Z^{k^*}} \\ v_I^k = \frac{Z^k v^k + Z^{k^*} v^{k^*}}{Z^k + Z^{k^*}} + sign\left(\frac{\partial \alpha^k}{\partial x},\right) \frac{P^{k^*} + P^k}{Z^k + Z^{k^*}} \end{cases} \tag{2}$$

where Z^k represents the acoustic impedance, *i.e.* $Z = \rho c$, where c is the speed of sound. The coefficients λ and μ_r are the relaxation velocity parameter and the dynamic compaction viscosity, respectively. They are associated to the relaxation terms that appear in the system to reproduce relaxation process behind shock and pressure waves in the two-phase flow, inducing a pressure and velocity equilibrium.
Writing $\lambda = \frac{1}{\varepsilon}$ and $\mu_r = \frac{1}{\varepsilon}$, the system can be formulated in a simplified notation, as follows:

$$\frac{\partial U}{\partial t} + \frac{\partial F(U)}{\partial x} = \frac{\partial U}{\partial t} + A(U)\frac{\partial U}{\partial x} = \frac{R(U)}{\varepsilon} \tag{3}$$

where U is the vector of conservative variables, $F(U)$ the flux vector and $R(U)$ the relaxation term. The reduced model, *i.e.* supposing $P_k = P_{k^*}$ and $v_k = v_{k^*}$, can be obtained using an asymptotic analysis that allows to find the solutions S, a subset of $\mathbb{R}^N$ of system (3) when $\varepsilon \to 0^+$:

$$W = \left\{U \in \mathbb{R}^N : R(U) = 0\right\} \tag{4}$$

As demonstrated by Murrone and Guillard [9] (see also [22, 17]), for each solution $U \in W$, we can compute a parametrization M such that, let $u = (\alpha_1, \rho_1, u, P, \alpha_2, \rho_2)^t \in \mathbb{R}^5$ the vector of primitives variables, the parametrization $M : u \to M(u)$ is defined as follows:

$$u \to U = M(u) = \begin{pmatrix} \alpha_1 \\ \rho_1 \\ u \\ P \\ \alpha_2 \\ \rho_2 \\ u \\ P \end{pmatrix}. \tag{5}$$

The reduced model of (3) is thus obtained by neglecting the terms of order ε:

$$\frac{\partial u}{\partial t} + PA(M(u))dM_u\frac{\partial u}{\partial x} = O(\varepsilon). \tag{6}$$

The term dM_u represents the Jacobian matrix that forms a basis of $\ker R'(M(u))$, moreover P is the projection over $\ker R'(M(u))$ in the direction of $Rng(M(u))$, that is the range of $R'(M(u))$. In particular, the projection P is obtained as inversion of the matrix $S = [dM_u^1, ..., dM_u^n, I^1, I^2]$, where $\left\{I^1, I^2\right\}$ is a basis of $Rng(R'(M(u)))$. The reduced model is the following:

$$\begin{cases} \dfrac{\partial \bar{\alpha}^1}{\partial t} & = -\vec{v}\cdot\nabla\alpha^1 + K\nabla(\vec{v}) \\ \dfrac{\partial \alpha^1\rho^1}{\partial t} + \nabla(\alpha^1\rho^1\vec{v}) & = 0 \\ \dfrac{\partial \alpha^2\rho^2}{\partial t} + \nabla(\alpha^2\rho^2\vec{v}) & = 0 \\ \dfrac{\partial \rho\vec{v}}{\partial t} + \nabla(\rho^k\vec{v}\otimes\vec{v} + P) & = \nabla\tau \\ \dfrac{\partial E}{\partial t} + \nabla(E + P) & = \nabla\tau\cdot\vec{v} \end{cases} \tag{7}$$

where $K = \alpha_1\alpha_2(\rho_2 c_2^2 - \rho_1 c_1^2)/(\alpha_1\rho_2 c_2^2 + \alpha_2\rho_1 c_1^2)$.
As explained in Abgrall [17], unfortunately, in the system (7), a nonconservative production appears in the vapor volume fraction equation. The difficulty, from a mathematical point of view, is that this term has no meaning in the case where v and K are simultaneously discontinuous. In this case, it is difficult

to derive a numerical scheme. However, in [17], a scheme that allow to overcome this problem has been proposed and it is used in this work. It is explained in the following section.

In the system (7), $\rho = \alpha_1\rho_1 + \alpha_2\rho_2$, P and $E = \alpha_1\rho_1 e_1 + \alpha_2\rho_2 e_2$ are the mixture density, pressure and energy, respectively. To close the system (7), we need an EOS for each pure fluid and for the mixture, permitting to define all the needed thermodynamic properties. In the case of SG EOS, the value of the mixture pressure is easily derived from the mixture energy and the density for each phase [23]. On the contrary, when the PR EOS is used, there is no explicit relation between the pressure and the energy, thus making more complex the computation of the mixture pressure.

2.2 Numerical Method

Here, we illustrate how obtaining a semi-discrete numerical approximation of the two-phase system including the viscous term (Eq. 1), following the same procedure of [6].

We describe this scheme in the framework of finite volume discretization with a Godunov solver, but the procedure can be easily adapted to other solvers. Let us define our time-space domain. At time t, the computational domain Ω is divided into a *constant* number of cells $\mathcal{C}_i =]x_{i-1/2}, x_{i+1/2}[$. In addition, each cell $\mathcal{C}_i$ is divided into a random subdivision $x_{i-1/2} = \xi_0 < \xi_1 < ... < \xi_{N(\omega)} = x_{i+1/2}$ (where ω is a random parameter).

In each subcell $]\xi_l, \xi_{l+1}[$, X^k is constant and so only one phase Σ_k can exist. Neglecting the source terms S of Eq.2, the integral form of Navier-Stokes equations for the space-time domain $\mathcal{C}_i \times [t, t+s]$ is equal to

$$\int_t^{t+s}\int_{\mathcal{C}_i} X\frac{\partial U}{\partial t} + \int_t^{t+s}\int_{\mathcal{C}_i} X\frac{\partial (F - F_v)}{\partial x}dx\,dt = 0 \tag{8}$$

The Godunov scheme is no longer applied on the mesh cells, but on the modified and non-uniform cells constructed according to the position of the interface.

The variable $\sigma_{i+1/2} = \sigma(U_i, U_{i+1})$ denotes the speed of the interface between the two cells $\mathcal{C}_i$ and $\mathcal{C}_{i+1}$. Remark that it is equal to zero, if the same phase is present into the cells, otherwise $\sigma_{i+1/2}$ coincides with the speed of propagation of the interface in the Riemann solution $(x,t) \to v_r(\frac{x}{t}; U_i, U_{i+1})$. Thus, assuming that between the times t^n and $t^{n+1} = (t+s)$, the interface $x_{i+1/2}$ moves at velocity $\sigma_{i+1/2}$, the cell $\mathcal{C}_i$ is not fixed, but it evolves in $\bar{\mathcal{C}}_i =](x_{i-1/2} + s\sigma_{i-1/2}), (x_{i+1/2} + s\sigma_{i+1/2})[$ (see Fig. 1). The cell may be either smaller or larger than the original ones $\mathcal{C}_i$, depending on the signs of the velocities $\sigma_{i+1/2}$. We denote with $F(U_L, U_R)$ the Godunov numerical flux between the states U_L and U_R, and with $F^{lag}(U_L, U_R)$ the flux across the contact discontinuity between the states U_L and U_R (see Fig. 2). As a consequence, we have:

$$F^{lag}(U_L, U_R) = F(U_{LR}^+) - \sigma(U_L, U_R)U_{LR}^+ = F(U_{LR}^-) - \sigma(U_L, U_R)U_{LR}^-$$

Considering Fig. 1, the previous integral (Eq.8), defined on the mesh cell $\mathcal{C}_i$, can be divided into three contributions, *i.e.* the integrals on *abb'* for the left boundary, the integral on *bcc'* for the right boundary and the Lagrangian internal cells.

Thus Eq.8 can be rewritten as

$$\int_{abb'} X\left[\frac{\partial U}{\partial t} + \frac{\partial (F - F_v)}{\partial x}\right]dx\,dt + \quad (I)$$

$$+ \sum_{l=2}^{N(\varpi)-2}\int_t^{t+s}\int_{\xi_l + s\sigma(U_i^l, U_i^{l-1})}^{\xi_{l+1} + s\sigma(U_i^l, U_i^{l+1})} X\left[\frac{\partial U}{\partial t} + \frac{\partial (F - F_v)}{\partial x}\right]dx\;dt + \quad (II)$$

$$+ \int_{dcc'} X\left[\frac{\partial U}{\partial t} + \frac{\partial (F - F_v)}{\partial x}\right]dx\;dt = 0 \quad (III)$$

Including the characteristic function X in derivative terms and applying the Godunov scheme, we obtain for each term, the solution at time $t+s$. For the boundary terms (I) and (III), it is important to remark that the domain where computing the integral is a triangle. At time t we have only one point (a) and thus the spatial integral is zero.

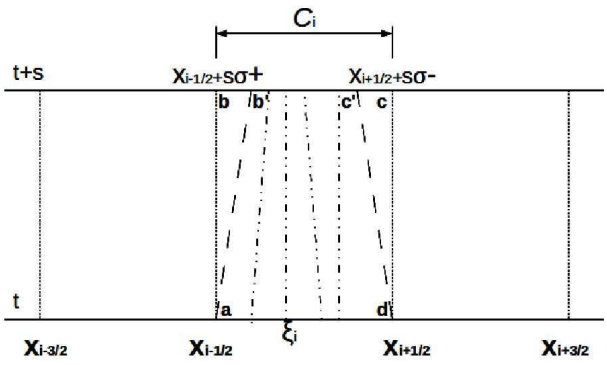


Figure 1: Subdivision of computational domain.

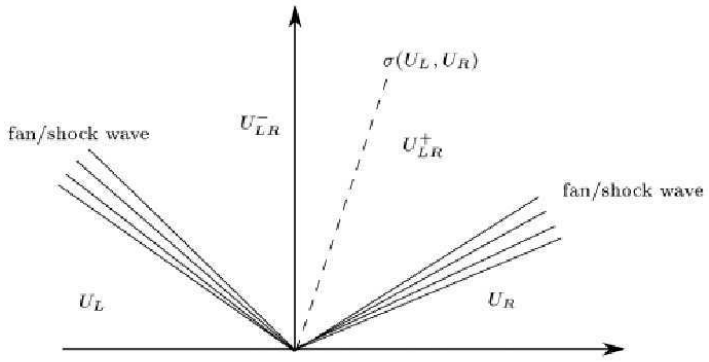


Figure 2: The various states in the Riemann problem between states U_L and U_R.

Remembering that the characteristic function obeys to the following property:

$$\sum_{l=0}^{N(\varpi)-1} \int_t^{t+s} \int_{\xi_l}^{\xi_{l+1}} \frac{\partial X}{\partial t}\, dx\, dt + \sum_{l=0}^{N(\varpi)-1} \int_t^{t+s} \int_{\xi_l}^{\xi_{l+1}} \sigma \frac{\partial X}{\partial x} dx\, dt = 0, \tag{10}$$

we can write for (I)

$$\begin{aligned}
&\int_{abb'} X \left[\frac{\partial U}{\partial t} + \frac{\partial (F - F_v)}{\partial x}\right] dx\, dt = \\
&\quad \int_{abb'} \left[\frac{\partial XU}{\partial t} + \frac{\partial X(F - F_v)}{\partial x}\right] dxdt - \int_{abb'} \left[U \frac{\partial X}{\partial t} + (F - F_v)\frac{\partial X}{\partial x}\right] dxdt = \\
&\quad \int_{x_{i-1/2}}^{x_{i-1/2}+s\sigma^+(U^+_{i-1},U^-_i,)} X(x, t+s)U(x, t+s)\, dx - sX(x_{i-1/2}, t)F(U^*_{i-1/2}) + \\
&\quad -sF^{lag}(U^+_{i-1}, U^-_i)[X]_{j=0} + \mathbf{sX(x_{i-1/2}, t)F_v(U^*_{i-1/2})} + \mathbf{sF_{vI}(U^+_{i-1}, U^-_i)[X]_{j=0}},
\end{aligned}$$

where $U^*_{i\pm 1/2}$ is the solution of the Riemann problem. In this work, no mass transfer is considered, then when a jump is considered, the viscous contribution is zero because there is not transfer of

viscous information. Similarly, the term (III) can be manipulated as follows

$$\int_{dcc'} X\left[\frac{\partial U}{\partial t}+\frac{\partial (F-F_v)}{\partial x}\right]dx\,dt=$$
$$\int_{dcc'}\left[\frac{\partial XU}{\partial t}+\frac{\partial X(F-F_v)}{\partial x}\right]dxdt-\int_{dcc'}\left[U\frac{\partial X}{\partial t}+(F-F_v)\frac{\partial X}{\partial x}\right]dxdt=$$
$$\int_{x_{i+1/2}}^{x_{i+1/2}+s\sigma^-(U_i^+,U_{i+1}^-,)} X(x,t+s)U(x,t+s)\,dx+sX(x_{i+1/2},t)F(U^*_{i+1/2})+$$
$$+sF^{lag}(U_i^+,U_{i+1}^-)[X]_{j=N(w)}-\mathbf{sX(x_{i+1/2},t)F_v(U^*_{i+1/2})}-\mathbf{sF_{vI}(U_i^+,U_{i+1}^-)[X]_{j=N(w)}}.$$

Concerning the internal terms (II), the integral becomes

$$\int_t^{t+s}\int_{\xi_j+s\sigma(U_i^{j-1},U_i^j)}^{\xi_{j+1}+s\sigma(U_i^l,U_i^{l+1})} X\left[\frac{\partial U}{\partial t}+\frac{\partial (F-F_v)}{\partial x}\right]dx\;\;dt=$$
$$\int_{\xi_j+s\sigma(U_i^{j-1},U_i^j)}^{\xi_{j+1}+s\sigma(U_i^l,U_i^{l+1})} X(x,t+s)U(x,t+s)\,dx-\int_{\xi_j}^{\xi_{j+1}} X(x,t)U(x,t)\,dx+$$
$$-s\left(F^{lag}(U_i^j,U_i^{j+1})[X]_j-F^{lag}(U_i^{j-1},U_i^j)[X]_{j-1},\right)+$$
$$+\mathbf{s}\left(\mathbf{F_v(U_i^j,U_i^{j+1})[X]_j-F_v(U_i^{j-1},U_i^j)[X]_{j-1},}\right).$$

Summing up all terms, dividing for s and taking the limit when $s\to 0$, we obtain the *semi-discrete* scheme

$$\frac{\partial}{\partial t}\left(\frac{1}{\triangle x}\int_{x_{i-1/2}}^{x_{i+1/2}} X(x,t)U(x,t)\,dx\right)+$$
$$+\frac{1}{\triangle x}\left(X(x_{i+1/2},t)F(U^*_{i+1/2})-X(x_{i-1/2},t)F(U^*_{i-1/2})\right)+$$
$$-\mathbf{\frac{1}{\triangle x}}\left(\mathbf{X(x_{i+1/2},t)F_v(U^*_{i+1/2})-X(x_{i-1/2},t)F_v(U^*_{i-1/2})}\right)=$$
$$=\frac{1}{\triangle x}\sum_{j=1}^{N(w)-1}\left(F^{lag}(U_i^j,U_i^{j+1})[X]_j-F^{lag}(U_i^{j-1},U_i^j)[X]_{j-1},\right)+$$
$$+\frac{1}{\triangle x}\left(F^{lag}(U_i^-,U_{i-1}^+)[X]_{j=0}-F^{lag}(U_i^+,U_{i+1}^-)[X]_{j=N(w)}\right)+$$
$$-\sum_{j=1}^{N(w)-1}\left(\mathbf{F_v(U_i^j,U_i^{j+1})[X]_j-F_v(U_i^{j-1},U_i^j)[X]_{j-1},}\right)+$$
$$-\mathbf{\frac{1}{\triangle x}}\left(\mathbf{F_v(U_i^+,U_{i+1}^-)[X]_{j=0}-F_v(U_i^+,U_{i+1}^-)[X]_{j=N(w)}}\right). \tag{11}$$

We may assume that two adjacent subcell contains different phases, so that

$$\sum_{j=1}^{N(w)-1}\left(F^{lag}(U_i^j,U_i^{j+1})[X]_j-F^{lag}(U_i^{j-1},U_i^j)[X]_{j-1}\right)=$$
$$=N(\omega)_{int}\left(F^{lag}(U_i^2,U_i^1)-F^{lag}(U_i^1,U_i^2)\right) \tag{12}$$

and

$$\sum_{j=1}^{N(w)-1} \left(\mathbf{F_v}(\mathbf{U_i^j}, \mathbf{U_i^{j+1}})[\mathbf{X}]_\mathbf{j} - \mathbf{F_v}(\mathbf{U_i^{j-1}}, \mathbf{U_i^j})[\mathbf{X}]_{\mathbf{j-1}}, \right) = \tag{13}$$
$$= N(\omega)_{int} \left(F_v(U_i^2, U_i^1) - F_v(U_i^1, U_i^2) \right).$$

2.3 Averaging procedure

Now, it is possible to apply to the discrete equations system (11), the same averaging procedure used for the system of partial differential equations of (1). Taking the mathematical expectancy of the semi-discrete scheme (Eq.11) for which we have:

$$\frac{\partial}{\partial t} \left(\frac{1}{\triangle x} \int_{x_{i-1/2}}^{x_{i+1/2}} X(x,t) U(x,t)\, dx \right) = \frac{\partial \alpha_i^{(1)} U_i^{(1)}}{\partial t} \tag{14}$$

and introducing the notation for the average number of internal interfaces,

$$\lambda_i = \mathcal{E} \left(\frac{N(\omega)_{int}}{\triangle x} \right),$$

the scheme can be rewritten as:

$$\begin{aligned}
&\frac{\partial \alpha_i^{(1)} U_i^{(1)}}{\partial t} + \frac{1}{\triangle x} \mathcal{E} \left(X(x_{i+1/2}, t) F(U^*_{i+1/2}) - X(x_{i-1/2}, t) F(U^*_{i-1/2}) \right) + \\
&-\frac{\mathbf{1}}{\triangle \mathbf{x}} \mathcal{E} \left(\mathbf{X}(\mathbf{x_{i+1/2}}, \mathbf{t}) \mathbf{F_v}(\mathbf{U^*_{i+1/2}}) - \mathbf{X}(\mathbf{x_{i-1/2}}, \mathbf{t}) \mathbf{F_v}(\mathbf{U^*_{i-1/2}}) \right) = \\
&+\frac{1}{\triangle x} \mathcal{E} \left(F^{lag}(U_i^-, U_{i-1}^+)[X]_{j=0} - F^{lag}(U_i^+, U_{i+1}^-)[X]_{j=N(w)} \right) + \\
&-\frac{\mathbf{1}}{\triangle \mathbf{x}} \mathcal{E} \left(\mathbf{F_{vI}}(\mathbf{U_i^+}, \mathbf{U_{i-1}^-})[\mathbf{X}]_{\mathbf{j=0}} \right) - \mathbf{F_{vI}}(\mathbf{U_i^+}, \mathbf{U_{i+1}^-})[\mathbf{X}]_{\mathbf{j=N(w)}} \\
&+\lambda_i \left(F^{lag}(U_i^2, U_i^1) - F^{lag}(U_i^1, U_i^2) \right) - \lambda_i \left((F_v(U_i^2, U_i^1) - F_v(U_i^1, U_i^2) \right).
\end{aligned} \tag{15}$$

The development of both conservative and non-conservatives terms have been fully described in [6, 17, 13], then here only final expressions of these terms are given for a second order scheme. We consider the cell boundary $i+1/2$ and focus on the fluxes available for fluid Σ_1. On this cell boundary, four instances may occur on the base of the phase present in the cell x_i and in the cell x_{i+1} (see Tab. 1). Thus, we can define the flux indicator

$$\beta_{i+1/2}^{(l,r)} = sign(\sigma(U_i^l, U_{i+1}^r)) = \begin{cases} 1 & if\ \sigma(U_i^l, U_{i+1}^r) \geq 0, \\ -1 & if\ \sigma(U_i^l, U_{i+1}^r) < 0 \end{cases}$$

and the corresponding probability to have the same phase or two different phases into the left and right cell of cell boundary $i+1/2$

$$\begin{aligned}
P_{i+1/2}(\Sigma_1, \Sigma_1) &:= P\left(X(x^-_{i+1/2}) = 1 \ and\ X(x^+_{i+1/2}) = 1 \right) = min\left(\alpha_i^{(1)},\ \alpha_{i+1}^{(1)} \right), \\
P_{i+1/2}(\Sigma_1, \Sigma_2) &:= P\left(X(x^-_{i+1/2}) = 1 \ and\ X(x^+_{i+1/2}) = 0 \right) = max\left(\alpha_i^{(1)} - \alpha_{i+1}^{(1)}, 0 \right), \\
P_{i+1/2}(\Sigma_2, \Sigma_1) &:= P\left(X(x^-_{i+1/2}) = 0 \ and\ X(x^+_{i+1/2}) = 1 \right) = max\left(\alpha_i^{(2)} - \alpha_{i+1}^{(2)}, 0 \right), \\
P_{i+1/2}(\Sigma_1, \Sigma_2) &:= P\left(X(x^-_{i+1/2}) = 0 \ and\ X(x^+_{i+1/2}) = 0 \right) = min\left(\alpha_i^{(2)},\ \alpha_{i+1}^{(2)} \right).
\end{aligned}$$

Following the MUSCL approach, we propose the following extension to a second-order approximation of the scheme. The system 15 can be written as follows:

$$\begin{aligned}
&\frac{\left(\alpha_i^{(1)}U_i^{(1)}\right)^{n+1}-\left(\alpha_i^{(1)}U_i^{(1)}\right)^{n}}{\Delta t}\\
&+\frac{\mathcal{E}\left(XF\right)_{i+1/2}-\mathcal{E}\left(XF\right)_{i-1/2}}{\Delta x}-\frac{\mathcal{E}\left(XF_v\right)_{i+1/2}-\mathcal{E}\left(XF_v\right)_{i-1/2}}{\Delta x}=\\
&=\mathcal{E}\left(F^{lag}\frac{\partial X}{\partial x}\right)_{i,bound}+\mathcal{E}\left(F^{lag}\frac{\partial X}{\partial x}\right)_{i,relax}+\\
&-\mathcal{E}\left(F_v\frac{\partial X}{\partial x}\right)_{i,bound}-\mathcal{E}\left(F_v\frac{\partial X}{\partial x}\right)_{i,relax}.
\end{aligned}\tag{16}$$

In the following, $U_{i\pm1/2,l}(resp.U_{i\pm1/2,r})$ are the vector of conservative variables on the left (resp. right) of the boundary cell $x_{i\pm1/2}$ after the MUSCL extrapolation, using a *minmod* limiter. Thus, all terms in the predictor-corrector scheme for a multiphase flows, take the following form

- *Conservative terms*

$$\begin{aligned}
\mathcal{E}\left(XF\right)_{i+1/2}&=P_{1+1/2}(\Sigma_1,\Sigma_1)F(U_{i+1/2,l}^{(1),n+1/2},U_{i+1/2,r}^{(1),n+1/2})\\
&+P_{1+1/2}(\Sigma_1,\Sigma_2)\left(\beta_{i+1/2}^{(1,2)}\right)^{+}F(U_{i+1/2,l}^{(1),n+1/2},U_{i+1/2,r}^{(2),n+1/2})+\\
&+P_{1+1/2}(\Sigma_2,\Sigma_1)\left(-\beta_{i+1/2}^{(2,1)}\right)^{+}F(U_{i+1/2,l}^{(2),n+1/2},U_{i+1/2,r}^{(1),n+1/2})
\end{aligned}\tag{17}$$

$$\begin{aligned}
\mathcal{E}\left(XF\right)_{i-1/2}&=P_{1-1/2}(\Sigma_1,\Sigma_1)F(U_{i-1/2,l}^{(1),n+1/2},U_{i-1/2,r}^{(1),n+1/2})\\
&+P_{1-1/2}(\Sigma_1,\Sigma_2)\left(\beta_{i-1/2}^{(1,2)}\right)^{+}F(U_{i-1/2,l}^{(1),n+1/2},U_{i-1/2,r}^{(2),n+1/2})+\\
&+P_{1-1/2}(\Sigma_2,\Sigma_1)\left(-\beta_{i-1/2}^{(2,1)}\right)^{+}F(U_{i-1/2,l}^{(2),n+1/2},U_{i-1/2,r}^{(1),n+1/2})
\end{aligned}\tag{18}$$

$$\begin{aligned}
\mathcal{E}\left(XF_v\right)_{i+1/2}&=P_{1+1/2}(\Sigma_1,\Sigma_1)F_v(U_{i+1/2,l}^{(1)},U_{i+1/2,r}^{(1)})\\
&+P_{1+1/2}(\Sigma_1,\Sigma_2)\left(\beta_{i+1/2}^{(1,2)}\right)^{+}F_v(U_{i+1/2,l}^{(1)},U_{i+1/2,r}^{(2)})+\\
&+P_{1+1/2}(\Sigma_2,\Sigma_1)\left(-\beta_{i+1/2}^{(2,1)}\right)^{+}F_v(U_{i+1/2,l}^{(2)},U_{i+1/2,r}^{(1)})
\end{aligned}\tag{19}$$

$$\begin{aligned}
\mathcal{E}\left(XF_v\right)_{i-1/2}&=P_{1-1/2}(\Sigma_1,\Sigma_1)F_v(U_{i-1/2,l}^{(1)},U_{i-1/2,r}^{(1)})\\
&+P_{1-1/2}(\Sigma_1,\Sigma_2)\left(\beta_{i-1/2}^{(1,2)}\right)^{+}F_v(U_{i-1/2,l}^{(1)},U_{i-1/2,r}^{(2)})+\\
&+P_{1-1/2}(\Sigma_2,\Sigma_1)\left(-\beta_{i-1/2}^{(2,1)}\right)^{+}F_v(U_{i-1/2,l}^{(2)},U_{i-1/2,r}^{(1)})
\end{aligned}\tag{20}$$

- *Non-conservative terms*

$$\begin{aligned}
\mathcal{E}\left(F^{lag}\frac{\partial X}{\partial x}\right)_i &= \mathcal{E}\left(F^{lag}\frac{\partial X}{\partial x}\right)_{bound} + \mathcal{E}\left(F^{lag}\frac{\partial X}{\partial x}\right)_{relax} = \\
&= +P_{1+1/2}(\Sigma_1,\Sigma_2)\left(\beta^{(1,2),n}_{i+1/2}\right)^{+} F^{lag}(U^{(1),n}_{i+1/2,l}, U^{(2),n}_{i+1/2,r}) + \\
&\quad -P_{1+1/2}(\Sigma_2,\Sigma_1)\left(\beta^{(2,1)}_{i+1/2}\right)^{+} F^{lag}(U^{(2),n}_{i+1/2,l}, U^{(1),n}_{i+1/2,r}) + \\
&\quad -P_{1-1/2}(\Sigma_1,\Sigma_2)\left(\beta^{(1,2)}_{i-1/2}\right)^{+} F^{lag}(U^{(1),n}_{i-1/2,l}, U^{(2),n}_{i-1/2,r}) + \\
&\quad +P_{1-1/2}(\Sigma_2,\Sigma_1)\left(\beta^{(2,1)}_{i-1/2}\right)^{+} F_{lag}(U^{(2)}_{i-1/2,l}, U^{(1)}_{i-1/2,r}) + \\
&+\sum_{N-1}^{l=1} max\left(0,\Delta\alpha^1_i\right)\left(F^{lag}(U^2_i,U^1_i) - max\sum_{N-1}^{l=1}\left(0,\Delta\alpha^2_i\right)F^{lag}(U^1_i,U^2_i)\right),
\end{aligned} \tag{21}$$

$$\begin{aligned}
\mathcal{E}\left(F_v\frac{\partial X}{\partial x}\right)_i &= \mathcal{E}\left(F_v\frac{\partial X}{\partial x}\right)_{bound} + \mathcal{E}\left(F_v\frac{\partial X}{\partial x}\right)_{relax} = \\
&= P_{1+1/2}(\Sigma_1,\Sigma_2)\left(\beta^{(1,2)}_{i+1/2}\right)^{-} F_{vI}(U^{(1)}_{i+1/2,l}, U^{(2)}_{i+1/2,r}) + \\
&\quad -P_{1+1/2}(\Sigma_2,\Sigma_1)\left(\beta^{(2,1)}_{i+1/2}\right)^{-} F_{vI}(U^{(2)}_{i+1/2,l}, U^{(1)}_{i+1/2,r}) + \\
&\quad -P_{1-1/2}(\Sigma_1,\Sigma_2)\left(\beta^{(1,2)}_{i-1/2}\right)^{+} F_{vI}(U^{(1)}_{i-1/2,l}, U^{(2)}_{i-1/2,r}) + \\
&\quad +P_{1-1/2}(\Sigma_2,\Sigma_1)\left(\beta^{(2,1)}_{i-1/2}\right)^{+} F_{vI}(U^{(2)}_{i-1/2,l}, U^{(1)}_{i-1/2,r}) + \\
&+max\left(0,\Delta\alpha^1_i\right)\left(F_v(U^2_i,U^1_i) - max\left(0,\Delta\alpha^2_i\right)F_v(U^1_i,U^2_i)\right),
\end{aligned} \tag{22}$$

where $\Delta\alpha^1_i = \alpha^1_{i+1/2,l} - \alpha^1_{i+1/2,r}$ and $\Delta\alpha^2_i = \alpha^2_{i+1/2,l} - \alpha^2_{i+1/2,r}$ are the limited slope of α^1 and α^2 in the cell C_i. The viscous fluxes F_v and F_{vI} are reconstructed by a backward difference on the base of flow direction. We consider that the cell boundary $i+1/2$ and the viscous fluxes for the momentum and energy equations are:

- momentum

$$F_v(U^{(k)}_{i+1/2,l}, U^{(k)}_{i+1/2,r}) = \begin{cases} \frac{4}{3}\mu\frac{u_{i+\frac{1}{2}} - u^{(k)}_{(r)i-1}}{(3/2)dx}\; if\; \sigma \geq 0 \\ \frac{4}{3}\mu\frac{u_{i+\frac{1}{2}} - u^{(k)}_{(l)i+2}}{(3/2)dx}\; if\; \sigma < 0 \end{cases} \tag{23}$$

- energy

$$F_v(U^{(k)}_{i+1/2,l}, U^{(k)}_{i+1/2,r}) = \begin{cases} \frac{4}{3}\mu u_{i+\frac{1}{2}}\frac{u^{(k)}_{i+\frac{1}{2}} - u^{(k)}_{(r)i-1}}{(3/2)dx}\; if\; \sigma \geq 0 \\ \frac{4}{3}\mu u_{i+\frac{1}{2}}\frac{u^{(k)}_{i+\frac{1}{2}} - u^{(k)}_{(l)i+2}}{3/2dx}\; if\; \sigma < 0 \end{cases}$$

- momentum

$$F_{vI}(U^{(k)}_{i+1/2,l}, U^{(k)}_{i+1/2,r}) = \begin{cases} \frac{4}{3}\mu \frac{u^{(k)}_{I(r)_{i+1}} - u^{(k)}_{I(r)_i}}{dx} \; if \; \sigma \geq 0 \\ \frac{4}{3}\mu \frac{u_{I(r)_i} - u^{(k)}_{I(r)_{i+1}}}{dx} \; if \; \sigma < 0 \end{cases} \tag{24}$$

- energy

$$F_{vI}(U^{(k)}_{i+1/2,l}, U^{(k)}_{i+1/2,r}) = \begin{cases} \frac{4}{3}\mu u^{(k)}_{I_{i+\frac{1}{2}}} \frac{u^{(k)}_{I(r)_{i+1}} - u^{(k)}_{I(r)_i}}{dx} \; if \; \sigma \geq 0 \\ \frac{4}{3}\mu u^{(k)}_{I_{i+\frac{1}{2}}} \frac{u^{(k)}_{I(r)_i} - u^{(k)}_{I(r)_{i+1}}}{dx} \; if \; \sigma < 0 \end{cases}$$

where

$$u^{(k)}_{i+\frac{1}{2}} = \begin{cases} u^{(k)}_{(r)_i} \; if \; \sigma \geq 0 \\ u^{(k)}_{(l)_{i+1}} \; if \; \sigma < 0 \end{cases}$$

$$u^{(k)}_{I_{i+\frac{1}{2}}} = \begin{cases} u^{(k)}_{(r)_{I_i}} \; if \; \sigma \geq 0 \\ u^{(k)}_{(l)_{I_{i+1}}} \; if \; \sigma < 0 \end{cases}$$

where l and r represent the left and right side. To obtain the predictor scheme, the solution is calculated at time $t = n + 1/2$ and in the corrector scheme the solution is calculated at the time $t = n + 1$, using the solution computed at the predictor step.

3 Asymptotic analysis of the numerical scheme

The scheme presented in Eq. 16 is a semi-discrete numerical approximation of the seven equation model for modeling a two-phase flow. Now, the aim is to obtain the semi-discrete scheme for the reduced five equations model in a 1D configuration, where viscous effects are considered, following the procedure described in [13]. If we set $\varepsilon_i = 1/\lambda_i$, the discrete scheme for the seven equations model can be formally rewritten as

$$\frac{\partial W}{\partial t} + \frac{G}{\triangle x} = \frac{R(W)}{\varepsilon_i}. \tag{25}$$

where $W = (\alpha^{(1)}, \alpha^{(1)}U^{(1)}, \alpha^{(2)}, \alpha^{(2)}U^{(2)})$, G is the sum of convective fluxes, viscous fluxes and *bound* lagrangian fluxes, and $R(W)$ are the relaxation terms. As explained in section 2.2, let us consider $\varepsilon \to 0$ searching for the solutions such that the relaxation terms could disappear:

$$\mathcal{W} = \left\{ W \;\; such \;\; that \;\; R(W) = 0 \Rightarrow \mathcal{E}\left(F^{lag}\frac{\partial X}{\partial x}\right)_{i,relax} = 0. \right\} \tag{26}$$

Flow Patterns	Left and Right States	Flux Indicator
Σ_1, Σ_2	$U_i^{(1)}, U_{i+1}^{(2)}$	$\left(\beta_{i+1/2}^{(1,2)}\right)^+$
Σ_1, Σ_1	$U_i^{(1)}, U_{i+1}^{(1)}$	1
Σ_2, Σ_1	$U_i^{(2)}, U_{i+1}^{(1)}$	$-\left(\beta_{i+1/2}^{(2,1)}\right)^+$
Σ_2, Σ_2	$U_i^{(2)}, U_{i+1}^{(2)}$	0
Σ_1, Σ_2	$F_v(U_i^{(1)}, U_{i+1}^{(2)})$	$\left(\beta_{i+1/2}^{(1,2)}\right)^+$
Σ_1, Σ_1	$F_v(U_i^{(1)}, U_{i+1}^{(1)})$	1
Σ_2, Σ_1	$F_v(U_i^{(2)}, U_{i+1}^{(1)})$	$-\left(\beta_{i+1/2}^{(2,1)}\right)^+$
Σ_2, Σ_2	$F_v(U_i^{(2)}, U_{i+1}^{(2)})$	0
	Interface Flux	
$\Sigma_1 - \Sigma_2$	$F^{lag}(U_i^{(1)}, U_{i+1}^{(2)})$	$\left(\beta_{i+1/2}^{(1,2)}\right)^-$
$\Sigma_1 - \Sigma_1$	$F^{lag}(U_i^{(1)}, U_{i+1}^{(1)})$	0
$\Sigma_2 - \Sigma_1$	$F^{lag}(U_i^{(2)}, U_{i+1}^{(1)})$	$-\left(\beta_{i+1/2}^{(2,1)}\right)^-$
$\Sigma_2 - \Sigma_2$	$F^{lag}(U_i^{(2)}, U_{i+1}^{(2)})$	0
$\Sigma_1 - \Sigma_2$	$F_{v_I}(U_i^{(1)}, U_{i+1}^{(2)})$	$\left(\beta_{i+1/2}^{(1,2)}\right)^+$
$\Sigma_1 - \Sigma_1$	$F_{v_I}(U_i^{(1)}, U_{i+1}^{(1)})$	0
$\Sigma_2 - \Sigma_1$	$F_{v_I}(U_i^{(2)}, U_{i+1}^{(1)})$	$-\left(\beta_{i+1/2}^{(2,1)}\right)^+$
$\Sigma_2 - \Sigma_2$	$F_{v_I}(U_i^{(2)}, U_{i+1}^{(2)})$	0

Table 1: The flow configurations at the cell boundary $i + 1/2$.

Hence, the final scheme for the five equation model in conservative variables is equal to:

$$\begin{cases} \dfrac{\partial \bar{\alpha}_2}{\partial t} = & FV_2 + \dfrac{\bar{\alpha}_1\bar{\alpha}_2}{\bar{\alpha}_2\bar{\rho}_1 a_1^2 + \bar{\alpha}_1\bar{\rho}_2 a_2^2}\left\{ \dfrac{SE_2}{\bar{\alpha}_2\bar{\rho}_2\beta_2} - \dfrac{u_2 SU_2}{\bar{\alpha}_2\bar{\rho}_2\beta_2} + \dfrac{\frac{{u_2}^2}{2} - \varepsilon_2 - \rho_2\kappa_2}{\bar{\alpha}_2\bar{\rho}_2\beta_2} M_2 + \right. \\ & \left. \dfrac{\rho_2^2\kappa_2 FV_2}{\bar{\alpha}_2\bar{\rho}_2\beta_2} - \dfrac{SE_1}{\bar{\alpha}_1\bar{\rho}_1\beta_1} + \dfrac{u_1 SU_1}{\bar{\alpha}_1\bar{\rho}_1\beta_1} - \dfrac{\frac{{u_1}^2}{2} - \varepsilon_1 - \rho_1\kappa_1}{\bar{\alpha}_1\bar{\rho}_1\beta_1} M_1 - \dfrac{\rho_1^2\kappa_1 FV_1}{\bar{\alpha}_1\bar{\rho}_1\beta_1} \right\} \\ \dfrac{\partial \alpha_k\bar{\rho}_k}{\partial t} = & M_k \\ \dfrac{\partial \rho u}{\partial t} = & SU_1 + SU_2 \\ \dfrac{\partial \rho E}{\partial t} = & SE_1 + SE_2 \end{cases} \tag{27}$$

where FV, M_k, SU and SE are the fluxes of vapor volume fraction equation, conservative mass equation, momentum equation and conservative energy equation, respectively and where:

$$\beta_i^k = \left(\frac{\partial \epsilon_i^k}{\partial P_i^k}\right)_{\rho_i^k} \quad and \quad \kappa_i^k = \left(\frac{\partial \epsilon_i^k}{\partial \rho_i^k}\right)_{P_i^k}$$

3.1 Thermodynamic closure

As we have previously mentioned, we deal with pure fluid and artificial mixture zone, thus the EOS must be able to describe the flow both in pure fluids and mixture zones.
In this section, first we describe two EOSs, *i.e.* the Stiffened Gas (SG) EOS and the Peng-Robinson (PR) EOS. Then, we build the mixture EOS using first the SG EOS for each phase and after the PR and the SG for the gas and the liquid phase, respectively.

3.1.1 Stiffened Gas EOS for pure fluid

The Stiffened Gas EOS is usually used for shock dynamics and its robustness for simulating two-phase flow with or without mass transfer has been amply demonstrated [6, 9, 10, 17, 23]. It can be written as follows:

$$P(\rho, e) = (\gamma - 1)(e - q)\rho - \gamma P_\infty, \tag{28}$$

$$e(\rho, T) = Tc_v + \frac{P_\infty}{\rho c_v} + q \tag{29}$$

$$h(T) = \gamma c_v T, \tag{30}$$

where p, ρ and e are the pressure, the density and the energy, respectively. The politropic coefficient γ is the constant ratio of specific heat capacities $\gamma = c_p/c_v$, P_∞ is a constant reference pressure and q is the energy of the fluid at a given reference state. Moreover, T, c_v and h are the temperature, the specific heat at constant volume and the enthalpy, respectively. The speed of sound, defined as $c^2 = (\frac{\partial P}{\partial \rho})_s$ can be computed as follows:

$$c^2 = \gamma \frac{P + P_\infty}{\rho} = (\gamma - 1)c_p T \tag{31}$$

where c^2 remains strictly positive (for $\gamma > 1$). It ensures the hyperbolicity of the system and the existence of a convex mathematical entropy [24].

3.1.2 *Peng-Robinson (PR) EOS for pure fluid*

Peng and Robinson (1976) proposed a cubic EoS of van der Waals type in the form:

$$p = \frac{RT}{v-b} - \frac{a}{v^2+2bv-b^2}. \tag{32}$$

where p and v denote respectively the fluid pressure and its specific volume, a and b are substance-specific parameters related to the fluid critical-point properties p_c and T_c and representative of attractive and repulsive molecular forces. To achieve high accuracy for saturation-pressure estimates of pure fluids, the temperature-dependent parameter a in Eq. (32) is expressed as

$$a = \left(0.457235 R^2 T_c^2/p_c\right) \cdot \alpha\left(T\right), \tag{33}$$

while

$$b = 0.077796 RT_c/p_c. \tag{34}$$

These parameters are not completely independent, since isothermal lines in the p-v plane should satisfy the thermodynamic stability conditions of zero curvature and zero slope at the critical point. Such conditions allow computing the critical compressibility factor $Z_c = (p_c v_c)/(RT_c)$ as the solution of a cubic equation. The correction factor α in Eq. (33) is given by

$$\alpha\left(T_r\right) = \left[1 + K\left(1 - T_r^{0.5}\right)\right]^2, \tag{35}$$

with

$$K = 0.378893 + 1.4897153\omega - 0.17131848\omega^2 + 0.0196554\omega^3. \tag{36}$$

The parameter ω is the fluid acentric factor. The other needed information to complete the thermodynamic model, namely the ideal-gas isochoric specific heat of the fluid, is approximated through a power law, *i.e.*,

$$c_{v,\infty}\left(T\right) = c_{v,\infty}\left(T_c\right)\left(\frac{T}{T_c}\right)^n \tag{37}$$

with n a fluid-dependent parameter. From thermodynamic rules, the energy equation can be expressed as:

$$e = e_c + \frac{c_{v,\infty}(T_c)}{(n+1)T_c^n}(T^{n+1} - T_c^{n+1}) - \frac{a}{8^{0.5}b}\left(\alpha(T) - T\frac{d\alpha(T)}{dT}\right) ln\left|\frac{V+b(1+2^{0.5})}{V+b(1-2^{0.5})}\right| \tag{38}$$

where e_c is an energy reference value. The speed of sound can be expressed as follows:

$$a^2 = \left(\frac{\partial P}{\partial \rho}\right)_T + \frac{1}{\rho^2}\frac{T}{c_v}\left(\frac{\partial P}{\partial T}\right)_\rho^2. \tag{39}$$

3.1.3 *SG EOS based mixture*

The EOS for the mixture can be easily obtained using the EOS of the single phases. In this section, let us consider the mixture obtained supposing a SG EOS for each phase. The starting point is the mixture energy equation:

$$\rho E = \alpha_1\rho_1 e_1 + \alpha_2\rho_2 e_2. \tag{40}$$

The energy of each phase, e_k, can be replaced by the Eq.(28), obtaining the mixture total energy as a function of the phase pressure. Under pressure equilibrium, we obtain the following expression for the pressure mixture:

$$P(\rho, e, \alpha_k) = \frac{\rho(E - \frac{\alpha_1\rho_1 q_1}{\rho} - \frac{\alpha_2\rho_2 q_2}{\rho}) - \left(\frac{\alpha_1\gamma_1 P_{\infty,1}}{\gamma_1 - 1} + \frac{\alpha_2\gamma_2 P_{\infty,2}}{\gamma_2 - 1}\right)}{\frac{\alpha_1}{\gamma_1 - 1} + \frac{\alpha_2}{\gamma_2 - 1}} \tag{41}$$

In this paper, the term q is supposed equal to zero for each phase.

3.1.4 *PR-SG EOS based mixture*

In this section, let us consider a mixture, obtained using the SG EOS for the liquid and the PR EOS for the gas. In the case of SG EOS (see section (3.1.1)), we showed how the pressure mixture can be easily obtained from the energy and the density of each phase. If a PR EOS is considered, it is not possible to formulate explicitly the pressure as a function of the energy and the density. Then, the procedure shown in section (3.1.3) for the SG EOS can not be used in this case.
Under pressure equilibrium, the following system of two equations is obtained:

$$\begin{cases} P_1(T_1, \rho_1) = P_2(T_2, \rho_2) \\ \rho E = \alpha_1\rho_1 e_1 + \alpha_2\rho_2 e_2. \end{cases} \tag{42}$$

where P_1 represents the pressure state computed for the phase 1 described by the PR EOS, and P_2 the pressure of the phase 2 described by SG EOS. Remark that in this case, the unknowns are T_1 and T_2. Replacing P_1 as a function of T_1 and ρ_1 using Eq. (32) and P_2 using Eq. (28) in the first equation of the system (42), the liquid temperature T_2 can be expressed as a function of the gas temperature T_1:

$$T_2 = \left[\frac{T_1 R_1}{\frac{1}{\rho_1} - b_1} - \frac{\alpha(T_1)a_1}{\frac{1}{\rho_1^2} + \frac{2b_1}{\rho_1} - b_1^2} + P_{\infty,2}\right] \frac{1}{(\gamma_2 - 1)\rho_2 c_{v,\infty_2}} \tag{43}$$

Replacing the energy e_k of each phase using Eq. (38) for e_1 and using Eq. (29) for e_2 in the mixture energy equation (second equation of the system (42)), we obtain:

$$\rho E = \alpha_1\rho_1 \left\{e_c + \frac{c_{v,\infty}(T_c)}{(n+1)T_c^n}(T_1^{n+1} - T_c^{n+1}) - \frac{a}{2\sqrt{2}b}\left(\alpha(T_1) - T_1\frac{d\alpha(T)}{dT}\right) ln\left|\frac{V + b(1+\sqrt{2})}{V + b(1-\sqrt{2})}\right|\right\} + \alpha_2\rho_2 \left[T_2 c_{v,\infty_2} + \frac{P_{\infty,2}}{\rho_2 c_{v,\infty_2}} - \right. \tag{44}$$

Now, by replacing T_2 in the Eq. (44) using the Eq. (43), it is possible to derive a relation between the gas temperature, T_1, and the mixture energy. This is a function $E = E(T_1)$ that depends exclusively by T_1. Solving iteratively Eq. (44) by using a Newton-Raphson method, the value of the gas temperature T_1 can be computed.
Once T_1 is obtained, the mixture pressure can be easily computed using Eq. (32).

4 Results

This section illustrates various results. First, the implementation of the PR equation of state is validated by running a monophasic shock tube where the liquid fraction is supposed very reduced, and by comparing with respect to well-known results in literature. In this case, the working fluid is the FC70 fluid, permitting to simulate a rarefaction shock wave in the tube for

some specific conditions of pressure and temperature. The aim of this test case is twofold, i) to validate the implementation of PR EOS and to check the robustness of the proposed numerical scheme. Secondly, a two-phase shock tube is considered where the interest of using a more complex equation of state with respect to a simpler one is determined for several operating conditions.

4.1 Validation

Let us consider the test case presented by Fergason et al. [25], where a rarefaction shock is observed in a single-phase shock tube configuration. This non-classical phenomenon has been observed numerically in literature [26, 15, 27], even if an experimental confirmation of the rarefaction shock wave still does not exist. Only an accurate EOS, such as the PR EOS, can describe a so particular gas thermodynamic behavior. For this reason, this test-case represents a good validation for checking the EOS implementation.
The shock tube is filled out with only one fluid, the FC70, but for numerical reasons, each chamber contains a very weak volume of fraction of water ($\alpha_l = 10^{-8}$). The left side is at a pressure of 10.766×10^5 Pa, with a density equal to $\rho = 470.398\ kg/m^3$, while the right one is at a pressure of 8.635×10^5Pa with a density equal to $\rho = 248.991\ kg/m^3$. The diaphragm is located at $x = 2.5$ m (the tube is long 5 m). The results obtained with DEM have been validated with the numerical results obtained with the *NZDG* code (see [15] for more details), comparing the profiles at a time of $t = 2.3$ ms. The Table 2 provides the fluid properties of FC70 and the corresponding PR EOS parameters, *i.e.* the fluid acentric factor ω and the n coefficient (see Eq. 37), taken from [28].

In Figure 3, the evolution of dimensionless (computed with respect to the critical point) pressure, density, velocity and Mach along the tube axis are shown. A non-classical discontinuity wave field displaying a rarefaction shock wave on $x = 1.8$ m (see Figure 3) and a compression shock wave on $x = 3.5$ m are observed. The results obtained with the DEM code and the *NZDG* code [15] display a perfect agreement.

Name	$M(Kg/mol)$	$T_c(K)$	$P_c(atm)$	$v_c(m^3/kg)$	ω	n
$FC70$	0.821	608.2	10.2	1.8544×10^{-3}	0.7584	0.4930

Table 2: Molecular weight M, critical temperature T_c, critical pressure P_c, critical specific volume v_c, acentric factor ω and n coefficient

4.2 Dodecane test-cases

In this section, let us consider a shock tube filled out with liquid dodecane on the left and with vapor dodecane on the right without mass transfer. In the first test-case, already shown in [11], the vapor operating conditions are far from the saturation curve. In order to evaluate the importance of using a more complex EOS, three others test cases have been considered, using the same operating conditions for the liquid dodecane, but with the vapor operating conditions closer to the saturation curve. These three conditions, reported in the Amagat diagram in figure 4, have been named as TC2, TC3, and TC4.

4.2.1 Original dodecane test-case

The shock tube is filled out with liquid dodecane on the left and vapor dodecane on the right, but for numerical reasons, each chamber contains a weak volume of the other fluid ($\alpha_k = 10^{-8}$).

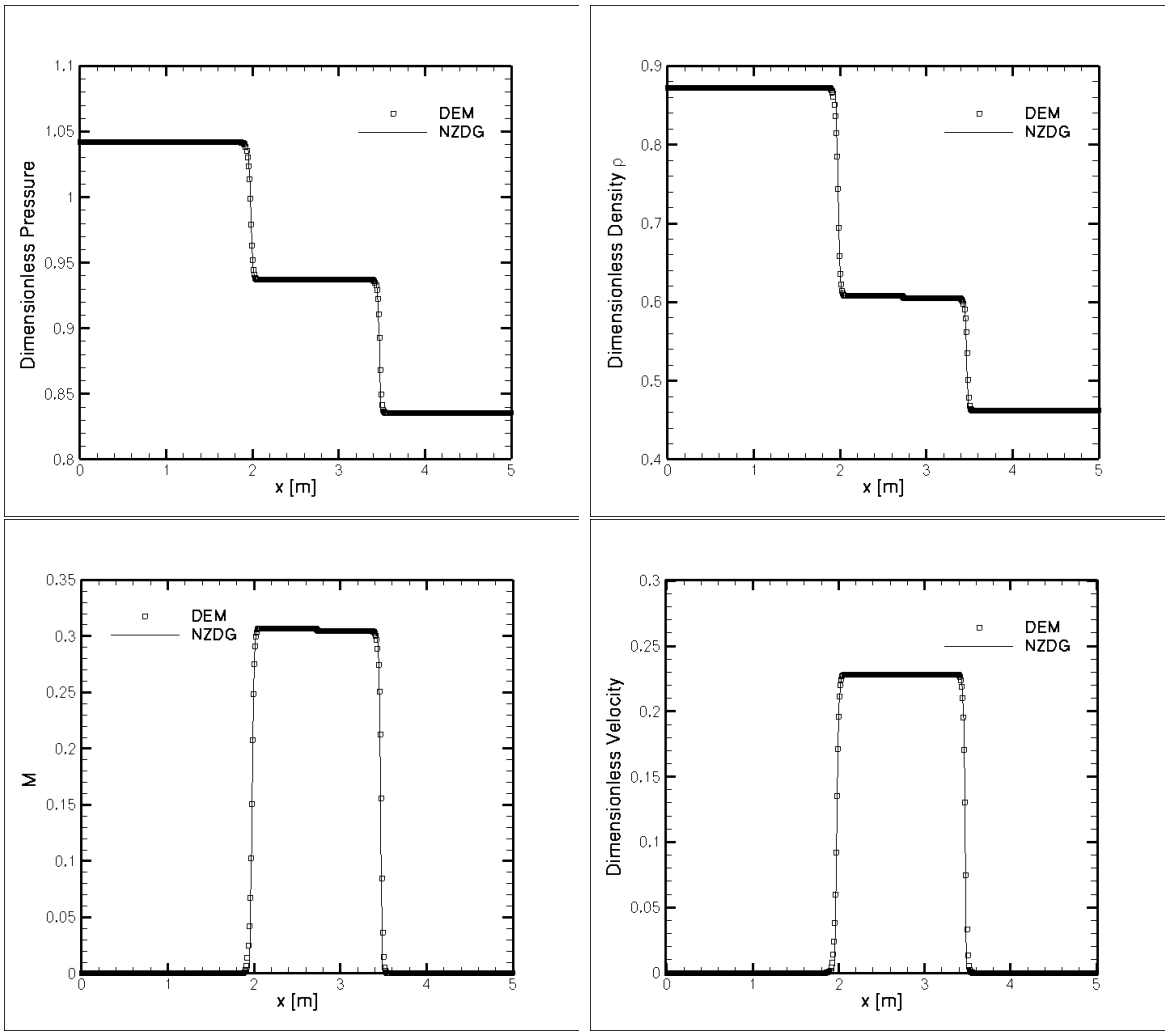


Figure 3: Comparison of the DEM results with the ones obtained with the *NZDG* code for a monophasic shock-tube flow in terms of pressure, density, Mach and velocity.

The left side is at a pressure of 10^8 Pa, with a density equal to $\rho_l = 500\ kg/m^3$, while the right one is set to an atmospheric pressure of 10^5 Pa with a density equal to $\rho_v = 2\ kg/m^3$. The diaphragm is located at $x = 0.75$ m (the tube is long 1 m) and the results are shown at a time of $t = 473\ \mu s$.

Two equations of state, *i.e.* PR and SG eos, have been considered. Also the exact solution for the SG EOS is reported (see Figure 5). The exact solution has been shown in [11] and it was calculated considering an Euler model coupled with the SG EOS. The comparison with exact solution of pressure and velocity profiles obtained with both the EOS shows a good agreement, showing that the viscous terms do not influence the final result. Anyway, this is coherent with the results shown in [13]. The Figure 5 illustrates a classical incident wave field, in which a rarefaction wave propagates from left to right through the liquid (see pressure, density and velocity profiles

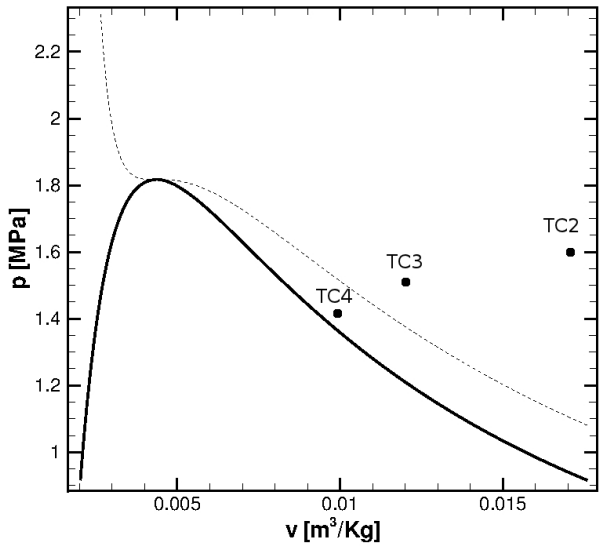


Figure 4: Dodecane saturation curve. The dash line is the isothermal curve $T = T_c$. TC2, TC3 and TC4 indicate the vapor operating conditions used in the second, third and fourth test cases, respectively.

in Figure 5 at $x < 0.2$ m), a contact discontinuity is moving from left to right (see density profile in Figure 5 at $x < 0.8$ m) and finally a shock wave propagates through the vapor (at $x < 0.85$ m in Figure 5).
The comparison between the two EOS does not display differences in term of pressure, velocity and density (Figure 5). On the contrary, the temperature profiles displays a difference between the SG profile and the PR profile. Let us focus to the zone for which $x > 0.75$ which corresponds to shock wave zone propagation though the vapor phase (Remark that for $x < 0.75$ the gas fraction is nearly equal to zero then the associated temperature has not a physical sense). If on one hand it is normal to obtain two different temperatures using two different EOS when imposing the same pressure and the same density, on the other hand a difference of about 300 K, between the two temperatures, is observed.
When cavitating flows should be considered, this difference can no more be negligible since that the cavitation term is activated according to the value of the local temperature.

4.2.2 Modified dodecane test-cases

Now, let us suppose to have the same liquid initial conditions of the previous test case, but to change the vapor initial conditions as in Table 3 (see Figure 4). The diaphragm is located at $x = 0.75$ m (the tube is long 1 m) and the results are shown at a time $t = 473$ μs. In this case, the profiles obtained by using the two EOS show evident differences not only in terms of temperature, but also in terms of density, pressure and velocity. In particular, an increasing density difference of about 7.7%, 36.4% and 42.9% is shown for the PR EOS with respect to SG EOS in the case TC2, TC3 and TC4, respectively. The same increasing difference can be observed for the temperature profiles. In particular, we observe that, instead of the first two cases (Figure 5-6), in the other ones, the temperature profile obtained with PR EOS is lower than the one obtained with SG EOS (see Figure 7-8). Observing that the density estimated

with PR is always higher than the SG density, this change is due to the pressure between the rarefaction wave and the compression shock. In fact, in the last two cases the pressure obtained by PR between $0.15 < x < 0.85$ is lower than the pressure obtained by SG EOS.

Finally, it is important to observe that getting closer to the saturation curve, *i.e.* from TC2 to TC4, the shock wave propagation velocity lowers, producing a change in the shock position. This can be observed in the velocity profiles (see Figure 5-7).

Conditions	TC2	TC3	TC4
$P[MPa]$	1.6	1.5	1.4
$V[m^3/Kg]$	0.017	0.012	0.01

Table 3: Pressure and specific volume for the TC2, TC3 and TC4 conditions

5 Conclusion and Future Work

In this paper, a semi-discrete scheme for the resolution of interface problems with viscosity has been presented, taking into account two different EOS for evaluating real gas effects. A reduced five equation model, under the hypothesis of pressure and velocity equilibrium, is used and discretized through the Discrete Equations Method (DEM). No mass and heat transfer is supposed. In this work, two EOS has been compared, the SG EOS and the PR EOS. In particular, the liquid phase is reproduced by the SG EOS, instead, the vapor phase is reproduced first with the SG EOS and, then, with the PR EOS. The PR EOS implementation has been validated by comparing the results obtained with the DEM code with the ones of a monophasic code [15]. In particular, the operating conditions and the working fluid have been chosen in order to reproduce a rarefaction shock wave. A perfect agreement has been obtained between the DEM and the NZDG code. Then, a two-phase shock tube (liquid and vapor Dodecane) has been considered, where the influence of using a different equation of state has been evaluated. As expected, for conditions closer to the saturation curve, the importance of considering a more complex equation of state, *i.e.* the PR EOS, increases. The implementation of the mass transfer terms is underway.

6 Acknowledgements

Remi Abgrall has been partially supported by the ERC Advanced Grant ADDECCO N. 226316.

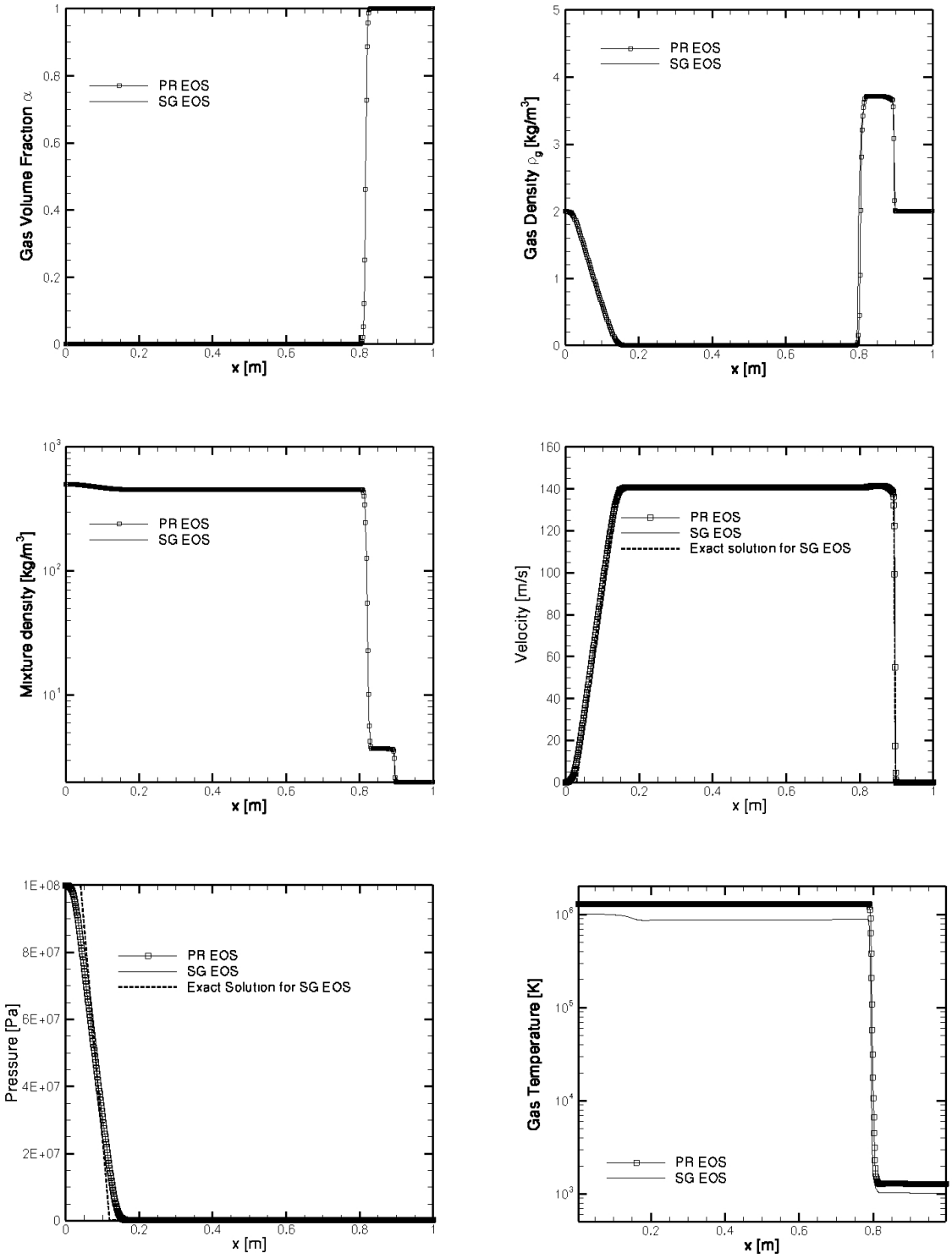


Figure 5: Vapor volume fraction, vapor density, mixture density, velocity, pressure and gas temperature profiles for the original dodecane test case [11].

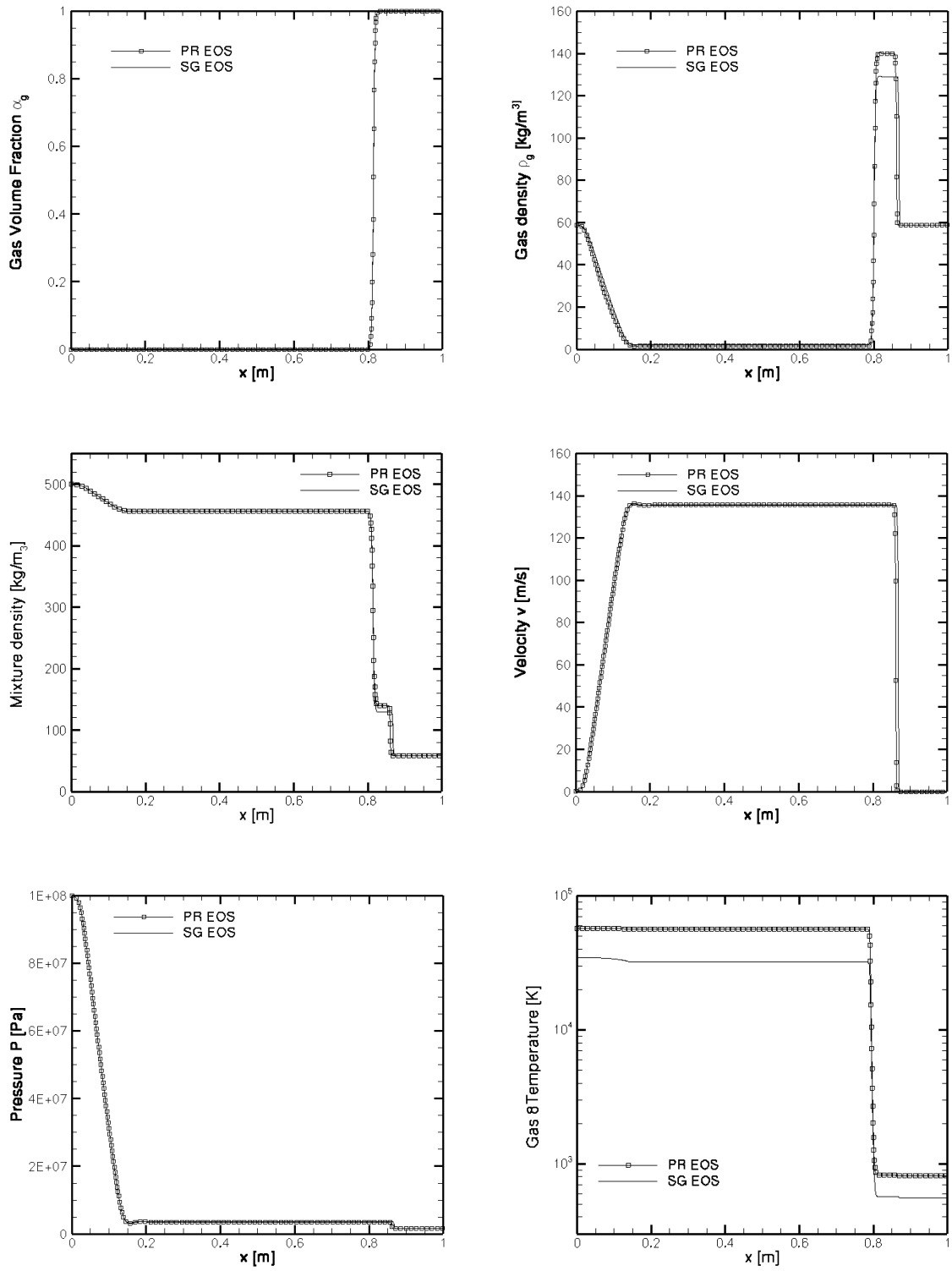


Figure 6: Vapor volume fraction, vapor density, mixture density, velocity, pressure and gas temperature profiles for TC2 test case.

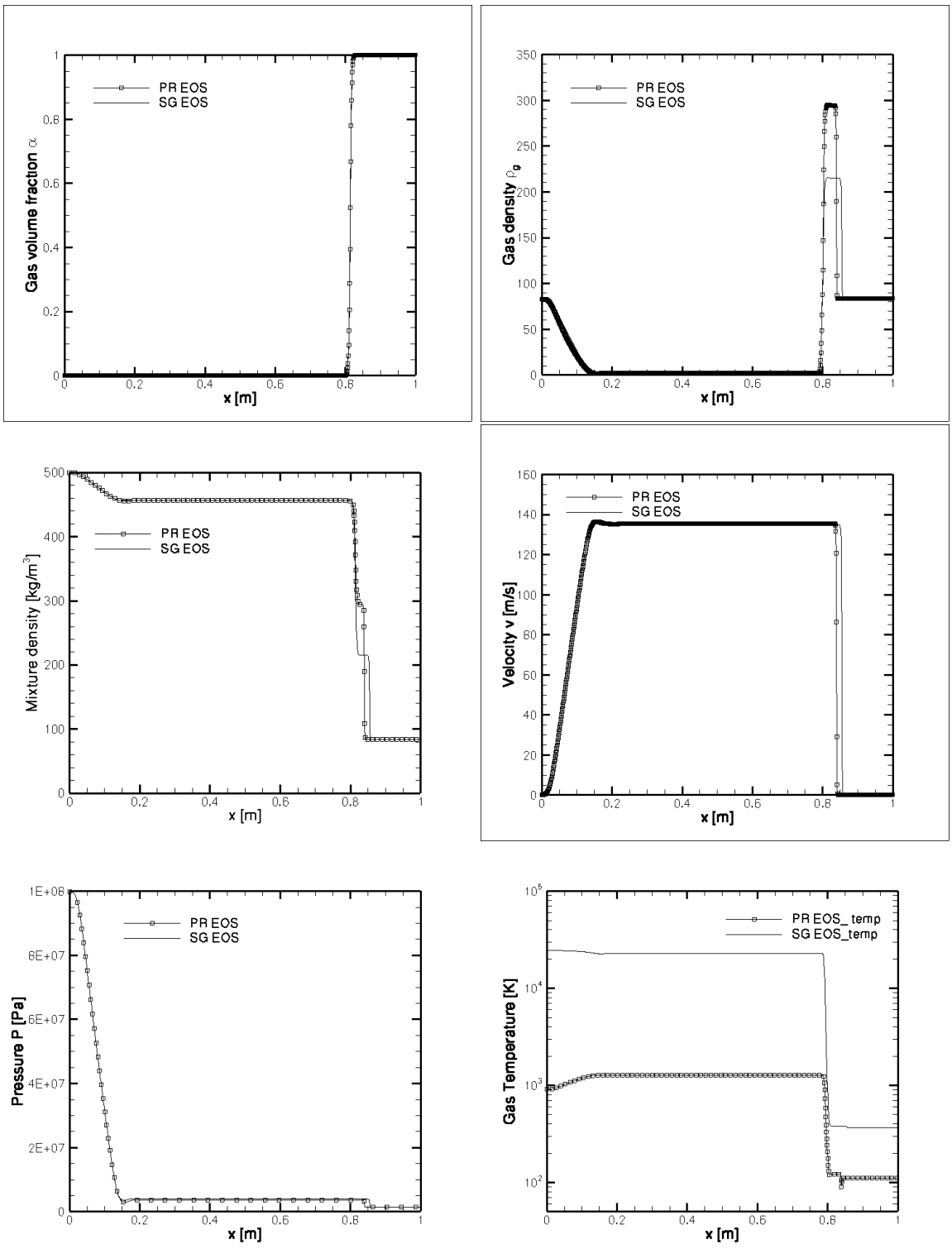


Figure 7: Vapor volume fraction, vapor density, mixture density, velocity, pressure and gas temperature profiles for TC3 test case.

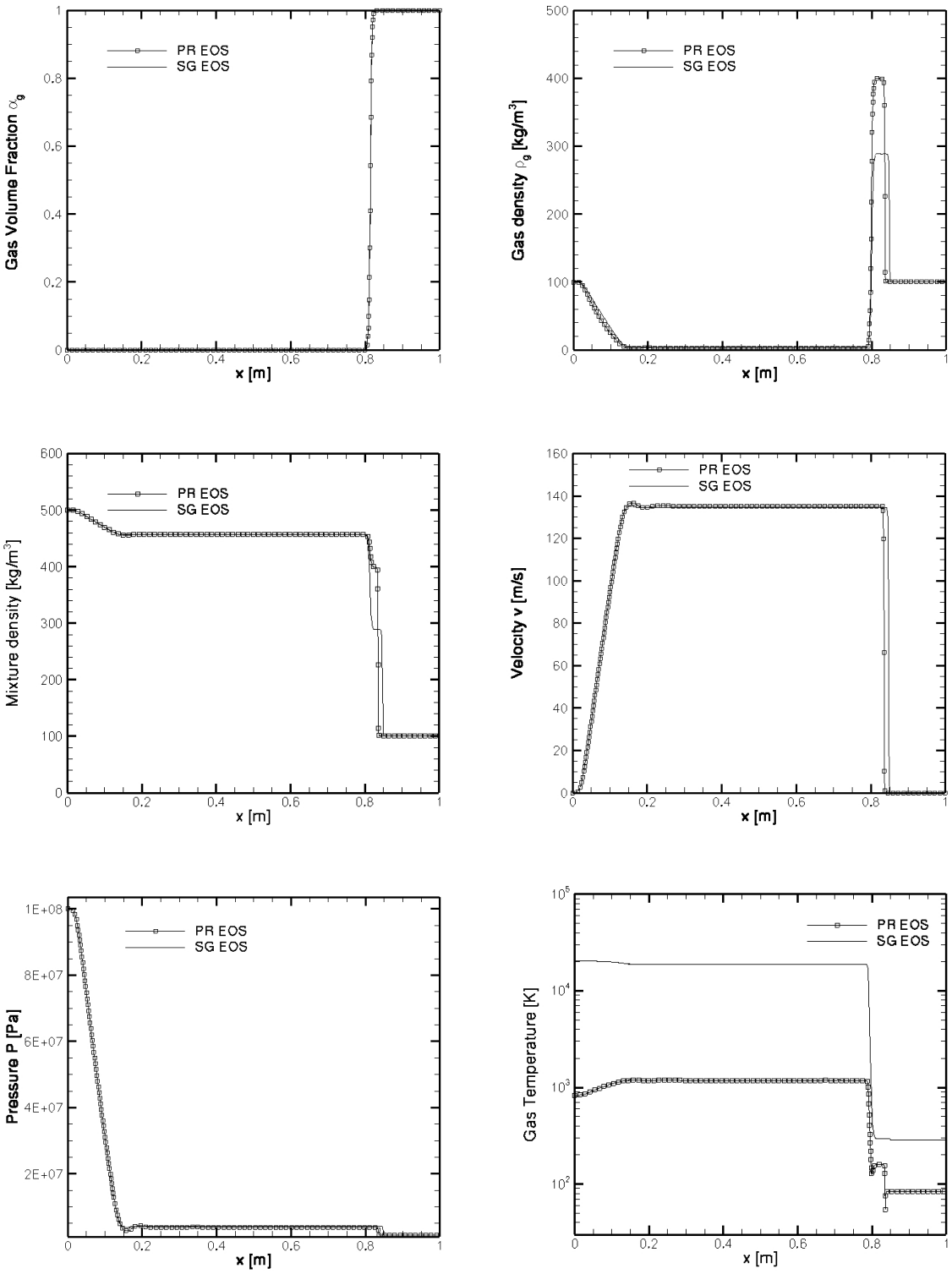


Figure 8: Vapor volume fraction, vapor density, mixture density, velocity, pressure and gas temperature profiles for TC4 test case.

References

[1] C. Farhat and F.X. Roux. A method of finite element tearing and interconnecting and its parallel solution algorithm. *International Journal for Numerical Methods in Engineering*, 32:1205–1227, 1991.

[2] G. Scovazzi, M.A. Christon, T.J.R. Hughes, and J.N. Shadid. Stabilized shock hydrodynamics: I. a lagrangian method. *Computer Methods in Applied Mechanics and Engineering*, 196:923–966, 2007.

[3] S. Osher and R.P. Fedkiw. Level set methods: An overview and some recent results. *Journal of Computational Physics*, 169:463–502, 2001.

[4] M.R. Bear and J.W. Nunziato. A two-phase mixture theory for deflagration to detonation transition (ddt) in reactive granular materials. *International Journal of Multhiphase Flow*, 12:861–889, 1986.

[5] R. Saurel and R. Abgrall. A multiphase godunov method for compressible multifluid and multiphase flows. *Journal of Computational Physics*, 150:425–467, 1999.

[6] R. Abgrall and R. Saurel. Discrete equations for physical and numerical compressible multiphase mixtures. *Journal of Computational Physics*, 186:361–396, 2003.

[7] G. Allaire, S. Clerc, and S. Kokh. A five-equation model for the simulation of interfaces between compressible fluids. *Journal of Computational Physics*, 181:577–616, 2002.

[8] F. Petitpas, J. Massoni, R. Saurel, E. Lapebie, and L. Munier. Diffuse interface model for high speed cavitating underwater systems. *International Journal of Multiphase Flow*, 35:747–759, 2009.

[9] A. Murrone and H. Guillard. A five equation reduced model for compressible two-phase flow problems. *Journal of Computational Physics*, 202:664–698, 2005.

[10] E. Goncalves and R.F. Patella. Numerical simulation of cavitating flows with homogeneous models. *Computers and Fluids*, 38:1682–1696, 2009.

[11] R. Saurel, F. Petitpas, and R. Abgrall. Modeling phase transition in metastable liquids. pplication to flashing and cavitating flows. *International Journal of Multiphase Flow*, 607:313–350, 2008.

[12] O. Lemetayer, J.Massoni, and R. Saurel. Elaboration des lois d'etat d'un liquide et de savapeur pour les modeles d'ecoulements diphasiques. *International Journal of Thermal Sciences*, 43:265–276, 2003.

[13] R. Abgrall and M.G. Rodio. Asymptotic Expansion of a Multiscale Numerical Scheme for Compressible Viscous Multiphase Flows. INRIA RR7920, 2012.

[14] P. Cinnella, P.M. Congedo, V. Pediroda, and L. Parussini. Sensitivity analysis of dense gas flow simulations to thermodynamic uncertainties. *Physics of Fluids*, 23:116101, 2011.

[15] P.M. Congedo, P. Colonna, C. Corre, J.A.S. Witteveen, and G. Iaccarino. Backward uncertainty propagation method in flow problems: Application to the prediction of rarefaction shock waves. *Computer Methods in Applied Mechanics and Engineering*, 213:314–326, 2012.

[16] R. Abgrall, P.M. Congedo, and S. Galera. A semi-intrusive deterministic approach to uncertainty quantifications in non-linear fluid flow problems. INRIA RR7820, 2011.

[17] R. Abgrall and V. Perrier. Asymptotic expansion of multiscale numerical scheme for compressible multiscale flow. *Society for Industrial and Applied Mathematics*, 5:84–115, 2006.

[18] R. A. Berry, R. Saurel, and O. LeMetayer. The discrete equation method (dem) for fully compressible, two-phaseflows in ducts of spatially varying cross-section. *Nuclear Engineering and Design*, 240:3797–3818, 2010.

[19] P. Cinnella, P. M. Congedo, V. Pediroda, and L. Parussini. Quantification of thermodynamic uncertainties in real gas flows. *International Journal of Engineering Systems Modelling and Simulation*, 2(1):12–24, 2010.

[20] P.M. Congedo, C. Corre, and J-M Martinez. Shape optimization of an airfoil in a bzt flow with multiple-source uncertainties. *Computer Methods in Applied Mechanics and Engineering*, 200:216–232, 2011.

[21] D.A. Drew and S.L. Passman. *Theory of Multicomponent Fluids*, volume 135. Applied Mathematical Sciences, Springer, New York, 1998.

[22] G.Perigaud and R. Saurel. A compressible flow model with capillary effects. *Journal of Computational Physics*, 209:139–178, 2005.

[23] R. Saurel, O. Le Metayer, J.Massoni, and S. Gavrilyuk. Shock jump relations for multiphase mixtures with stiff mechanical relaxation . shock waves. *Shock Waves*, 16(3):209–232, 2007.

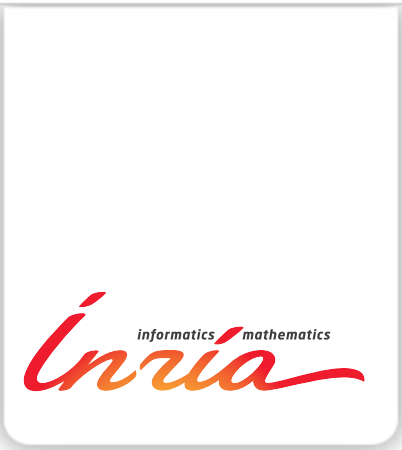
[24] A. Harten, P.D. Lax, C.D. Levermore, and W. Morokoff. Convex entropies and hyperbolicity for general euler equations. *SIAM Journal of Numerical Analysis*, 35(6):2117–2127, 1998.

[25] S. H. Fergason, T. L. Ho, B. M. Argrow, and G. Emanuel. Theory for producing a single-phase rarefaction shock wave in a shock tube. *Journal of Fluid Mechanics*, 445:37–54, 2001.

[26] P. A. Thompson and K. C. Lambrakis. Negative shock waves. *Journal of Fluid Mechanics*, 60:187, 1973.

[27] P. Colonna, A. Guardone, and N. R. Nannan. Siloxanes: a new class of candidate bethezel'dovich-thompson fluids. *Phys. Fluids*, 19(8):1–12, 2006.

[28] A. Guardone and B. Argrow. Nonclassical gasdynamic region of selected fluorocarbons. *Physics of Fluids*, 17:116102(17), 2005.



RESEARCH CENTRE
BORDEAUX – SUD-OUEST

351, Cours de la Libération
Bâtiment A 29
33405 Talence Cedex

Publisher
Inria
Domaine de Voluceau - Rocquencourt
BP 105 - 78153 Le Chesnay Cedex
inria.fr

ISSN 0249-6399